Theoretical Study of the Metal Oxidation Reaction Ti + O_2 → TiO + O: Ab Initio Calculation of the Potential Energy Surface and Classical Trajectory Analysis

Hideo Sakurai and Shigeki Kato*

Department of Chemistry, Graduate School of Science, Kyoto University, Kitashirakawa, Sakyo-ku, Kyoto 606-8502, Japan

Received: December 18, 2001; In Final Form: February 25, 2002

The oxidation reaction of the ground-state Ti(^{3}F) by the O_2 molecule has been studied theoretically. The 1^1A′ and 1^3A′ global potential energy surfaces (PESs) were calculated at the multireference configuration interaction level. The analytical PES for the 1^1A′ state is constructed on the basis of about 700 ab initio energies. Quasi-classical trajectory calculations are performed to obtain the product translational, rotational, and vibrational energy distributions as well as the lifetime of the collision complex. The primary reaction mechanism is assigned to the inserted/fast dissociation mechanism because the lifetime of the collision complex is short. The relative translational and rotational energy distributions are slightly hotter than those from the statistical prediction, reflecting a short-lived collision complex.

1. Introduction

The oxidation reactions of transition metals have been extensively studied because of their importance in understanding the mechanisms of corrosion and catalysis. Experimentally, Ritter and Weisshaar measured the rate constants for reactions of early transition metals Sc, Ti, and V in their ground electronic states with oxidants such as NO, O_2, and N_2O by monitoring the laser-induced fluorescence (LIF) of metal atoms in a fast-flow reactor.[1,2] They found that the depletion rates were very slow compared to those of of metal cations, indicating that there exists an entrance barrier on the potential energy surface (PES), and they interpreted the experimental results in terms of an electron-transfer mechanism. Clemmer, Honma, and Koyano[3] measured the LIF for the reactions of the excited-state Ti atom and obtained higher metal oxidation rate constants than those of the ground state, which seems to support the validity of the electron-transfer mechanism. Honma and co-workers carried out further experiments on Cr, Co, and Ni atoms with various oxidants to obtain general insight into the mechanism of transition metal oxidation reactions.[4−7] For the late transition metals Co and Ni, it was found that the oxidation reactions did not proceed, and only the quenching of excited metal atoms to the ground state by oxidants occurred.

Despite those experimental studies, theoretical work pertaining to the transition metal oxidation reactions is rather limited. Blomberg et al.[8] was the first to carry out ab initio calculations of NiO_2 and Ni_3O_2 to explore the mechanism of O_2 dissociation on Ni surfaces. Recently, several theoretical calculations of the PESs have been reported. Pápai et al.[9] examined the C−O bond dissociation of CO_2 caused by the Ti atom using density functional theory (DFT). The reaction was found to proceed without a potential barrier, which was explained by the attractive interaction between Ti 3d and CO_2 antibonding π* orbitals and the Ti 3d−4s hybridization that reduced the repulsive interaction between the Ti 4s and CO_2 σ orbitals. Stirling[10] performed DFT calculations to investigate the reaction mechanism of ground-state early transition metals with N_2O. The importance of two-way electron transfer was pointed out in interpreting the reaction mechanism; one electron is transferred from the metal 3d and later the 4s − 3d hybrid orbitals toward the lowest unoccupied orbital of N_2O, which weakens the N−O bond, and another electron transfer is from the highest occupied orbital of N_2O to the empty metal 3d orbital, which forms the metal−O bond.

In the present work, we have studied the dynamics of the oxidation reaction of the ground-state Ti by an O_2 molecule,

$$\mathrm{Ti}(^3\mathrm{F}) + \mathrm{O_2}(^3\Sigma) \rightarrow \mathrm{TiO}(^3\Delta) + \mathrm{O}(^3\mathrm{P}) \qquad \Delta H^\circ_{298} = -39.3 \pm 2.3 \text{ kcal/mol} \quad (1)$$

Three spin states (i.e., singlet, triplet, and quintet) can be involved in this reaction. However, considering that the entrance barrier is formed by the avoided crossing between the two states corresponding to the reactant and the side-on intermediate, only the 1^1A′ and 1^3A′ states seem to be responsible for the reaction because the two lowest states for the side-on complex are the 1^3A_1 and 1^1A_1 and the quintet states are at least 1.5 eV higher in energy than the lowest 1^3A_1. Note that the 1^1A_1 side-on complex is above the 1^3A_1 by only 0.2 eV.

We have carried out ab initio electronic structure calculations of the 1^1A′ and 1^3A′ PES to explore the reaction mechanism. A global PES for the 1^1A′ state is constructed for use in dynamics calculations. Quasi-classical trajectory (QCT) calculations have been further performed to estimate the reaction rate and product energy distributions. The role of side-on and inserted intermediates on the reaction dynamics has been examined by comparing the dynamics calculation results with those from the statistical assumption. To our knowledge, dynamics calculations for transition metal oxidation reactions in the gas phase are virtually nonexistent.

The organization of the article is as follows. In section 2, the results of ab initio calculations for the PESs are shown along with the computational details. The method for constructing an analytical PES is also described. Section 3 presents the results

* Corresponding author. E-mail: shigeki@kuchem.kyoto-u.ac.jp.

10.1021/jp014568l CCC: $22.00
Published on Web 03/29/2002

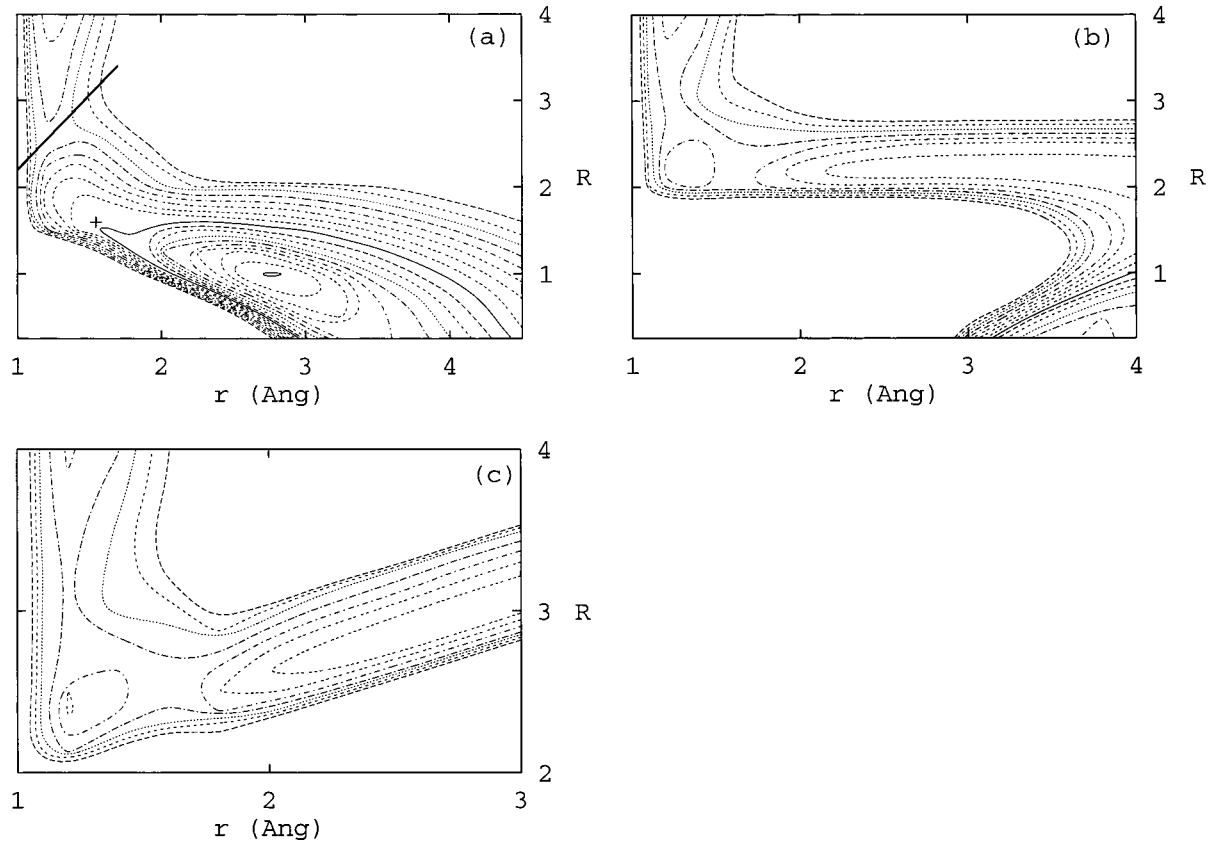

Figure 1. Contour plot of $1^1A'$ MRCI TiO_2 PES. Contour spacing is 0.5 eV. Distances r and R are given in Å. (a) $\theta = 90°$. The crossing seam between the 1^1B_2 and 1^1A_1 states is given by a solid line. + designates the position of the side-on complex. (b) $\theta = 45°$. (c) $\theta = 5°$.

of QCT calculations on the $1^1A'$ surface. The concluding remarks of this article are briefly summarized in section 4.

2. Potential Energy Surfaces

A. Ab Initio Calculations. The PESs of TiO_2 were calculated by the internally contracted multireference configuration interaction (MRCI) method[11] with the complete active-space self-consistent field (CASSCF) reference configurations. The CASSCF active space consists of 10 orbitals that correspond to the 4s and 3d orbitals of Ti and the π and π^* orbitals of O_2 in the reactant region. These orbitals are correlated to the 4s, nonbonding 3d, σ, σ^*, π, and π^* of TiO and two 2p orbitals of the O atom in the product region. Ten electrons are distributed among those active orbitals. For the Ti atom, the Wachters (14s9p5d)/[8s4p2d] basis set[12] supplemented with a set of diffuse d function whose exponent is 0.072[13] is used. To represent the anionic state of the O atom, a set of diffuse p functions with the exponent equal to 0.059 is added to the Huzinage−Dunning−Raffenetti (9s5p1d)/[3s2p1d] basis set[14] for the O atom.

We adopted the Jacobi coordinate system (R, r, θ) in describing the reaction system, where R, r, and θ denote the distance between Ti and the center of mass of O_2, the O−O internuclear distance, and the angle between the vectors **R** and **r**, respectively. We first carried out MRCI calculations at 785 points in the geometry range $2.0 \le R \le 4.0$ Å, $1.0 \le r \le 4.0$ Å, and $\theta = 5$, 15, 30, 45, 60, 75, and 90°. The electronic configurations whose coefficients are larger than 0.1 in the CASSCF wave function were chosen as the reference configurations of MRCI calculations. All the electronic structure calculations were carried out with the computer program MOLPRO 98.1.[15]

We show the $^1A'$ MRCI PES at three angles, $\theta = 90$, 45, and 5°, in Figure 1. For $\theta = 90°$, the 1^1B_2 state is lower than the 1^1A_1 state in the reactant region and crosses with the 1^1A_1 in the region between the reactant and side-on intermediate, as seen in Figure 1a. Because the number of grid points is not sufficient to represent a cusp along the crossing seam, we connected the energies on the 1^1B_2 and 1^1A_1 surfaces smoothly in Figure 1a. The minimum-energy crossing point is located at $R = 2.41$ Å and $r = 1.21$ Å, with the energy of 0.86 eV measured from the reactant. We can find two minima on the PES; one corresponds to the side-on intermediate ($R = 1.62$ Å, $r = 1.56$ Å) and the other, to the inserted one ($R = 1.03$ Å, $r = 2.79$ Å). In the side-on intermediate, the electron transfers from the Ti 3d orbitals to the O_2 π^*orbital and from the O_2 π orbital to the Ti 3d orbitals are observed. The 3d−4s hybridization on Ti was also found. The energy of the side-on structure is calculated to be −2.15 eV, which is measured from the reactant energy. In the inserted intermediate, the O−O bond is completely broken, and each O atom is bonded to Ti (i.e., the inserted dioxide). This is the most stable point on the PES, with an energy of −6.60 eV as predicted by Ramana and Phillips.[16] The barrier height from the side-on intermediate to the inserted one is low, 0.45 eV, and the differences between the side-on, −2.146 eV, and the middle barriers, −1.694 eV, are given in Table 1.

Figure 1b shows the PES at $\theta = 45°$. In C_s symmetry, the entrance barrier is formed by the avoided crossing between the 1^1B_2 and 1^1A_1 states, and its height is gradually lowered with decreasing θ. The energies of side-on and inserted intermediates become unstable upon reducing the symmetry from C_{2v} to C_s. Although the repulsive interaction between the Ti 3d and O_2 π orbitals becomes small with decreasing θ, the attractive interac-

TABLE 1: Geometries and MRCI Relative Energies of Stationary Points[a]

	R(OO)	R(TiO)[b]	R(TiO)	E(eV), $CI > 0.1$[c]	E(eV), $CI > 0.03$[d]
		$^1A'$			
reactant	1.2075[e]	∞	∞	0[f]	0[g]
barrier (perp.)	1.21	2.48	2.48	0.863	0.670
barrier (col.)	1.20	3.80	2.60	0.655	0.344
side-on	1.56	1.79	1.79	−2.146	−2.443
end-on	1.29	3.14	1.85	−0.654	−0.681
mid. barrier[h]	1.80	1.75	1.75	−1.694	−2.211
inserted	2.79	1.73	1.73	−6.592	−6.771
product	∞	∞	1.620[e]	−2.161	−1.803
		$^3A'$			
barrier (perp.)	1.22	2.40	2.40	0.954	0.779
barrier (col.)	1.21	3.44	2.23	0.670	0.519
side-on	1.44	1.84	1.84	−2.760	−2.775
end-on	1.29	3.14	1.85	−1.248	−1.353
inserted	3.00	1.80	1.80	−4.682	−4.397

[a] Bond distances are in Å and energies are in eV. [b] Dissociating TiO bond. [c] Thereshold of 0.1. [d] Thereshold of 0.03. [e] Ref 20. [f] Total energy is −998.495655 hartree. [g] Total energy is −998.517918 hartree. [h] The potential barrier between the side-on and inserted intermediate.

tions between Ti 3d and O_2 π and π^* are also reduced. Thus, the PES features in C_s symmetry is characterized by the variations of those repulsive and attractive interactions with the angle θ.

Figure 1c is shown for the angle $\theta = 5°$. In collinear geometry, the lowest state is $1^1\Sigma$, which undergoes the avoided crossing with $2^1\Sigma$ to form the entrance barrier. Note that the $2^1\Sigma$ is correlated to the $Ti^+ + O_2^-$ asymptote at the reactant. The entrance barrier is located at $R = 3.20$ Å and $r = 1.20$ Å, with the height of 0.66 eV indicating that the transition state has collinear geometry. As seen in Figure 1c, there is a shallow well with a depth of 0.65 eV at $R = 2.49$ Å and $r = 1.29$ Å, which corresponds to the end-on intermediate. The geometries and energies of stationary points on the $1^1A'$ surface are summarized in Table 1.

The PES for the 1^3A_1 state is shown in Figure 2. In C_{2v} symmetry, the lowest states are the 1^3B_2 in the reactant region and the 1^3A_1 for the side-on intermediate, as in the case of singlet PES. However, the inserted complex has B_2 symmetry; therefore, there are two crossing seams on the PES, as shown in Figure 2a. The energy at the minimum-energy crossing point between the reactant state and the side-on complex is calculated to be 0.95 eV, which is slightly higher than the corresponding value for the singlet state, 0.86 eV. The geometries and energies of the triplet side-on and inserted complexes are included in Table 1. The feature of the PES at $\theta = 5°$ shown in Figure 2b resembles that of the singlet PES. The lowest state is $^3\Sigma$, and the entrance barrier height is 0.67 eV at $R = 1.22$ Å and $r = 2.32$ Å. An end-on intermediate with a well depth of 1.25 eV is also observed. Considering that the barrier height of the $1^3A'$ state is very close to that of the $1^1A'$ state, the contribution from the triplet channel to the oxidation reaction seems to be similar to that from the singlet channel. We therefore examine the reaction dynamics proceeding on the singlet PES from this point forward.

Ritter and Weisshaar[1,2] estimated the activation energy for reaction 1 from the measured rate constant at 300 K. They fit the rate constant to the Arrhenius equation, $k(T) = A \exp(-E_{act}/RT)$, assuming the hard-sphere collision rate constant as the frequency factor A, and obtained the maximum value of 3.1 kcal/mol for E_{act}. As shown above, the present MRCI calculations gave an entrance-barrier height of 0.655 eV =15.1 kcal/mol for collinear geometry, which is much higher than the experimental estimate. Furthermore the reaction exothermicity is 2.16 eV, which is larger than the experimental value, 1.72 eV, obtained from the difference of bond dissociation energies of TiO and O_2.

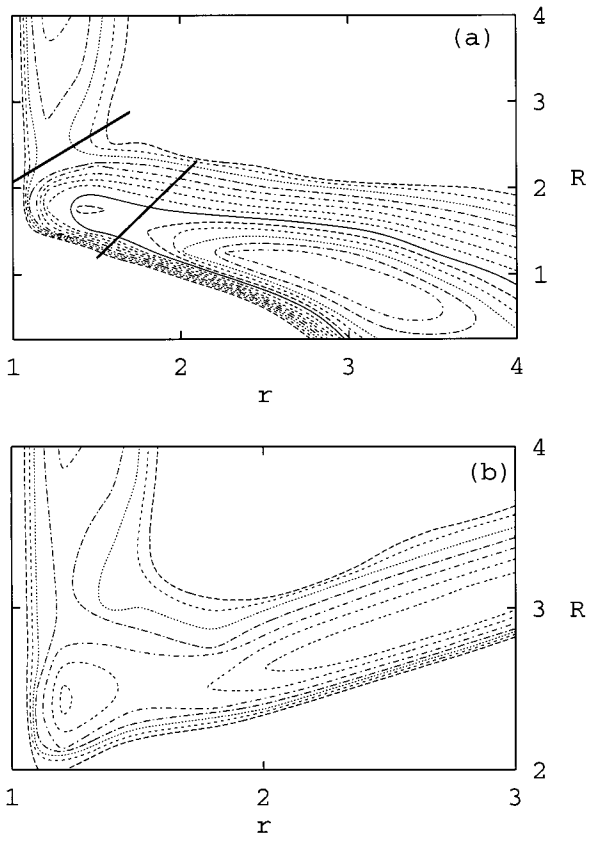

Figure 2. Contour plot of $1^3A'$ MRCI TiO_2 PES. Contour spacing is 0.5 eV. (a) $\theta = 90°$. Solid lines are crossing seams. (b) $\theta = 5°$.

Because it can be considered that these discrepancies between the calculated and experimental values are due to the insufficient treatment of the dynamic electronic correlation effect, we repeated the calculations for the critical geometries on the PESs in Figures 1 and 2, reducing the threshold for the configuration selection in MRCI calculations. Table 1 includes the energies obtained by the calculations with a threshold of 0.03 for configuration selection from the CASSCF wave function. We can see that the entrance barrier height is lowered to 0.344 eV= 7.9 kcal/mol and that the reaction exothermicity, 1.80 eV, is very close to the experimental value. The side-on and inserted intermediates are also stabilized by 0.29 and 0.18 eV, respectively.

B. Analytic Potential Energy Function. As mentioned above, the MRCI calculations with a threshold of 0.03 are desirable for constructing the PES. However, it is computationally too demanding for us to carry out the MRCI calculations at many grid points with this threshold value because the number of contracted configuration state functions (CSFs) becomes very large, $(1.2-2.3) \times 10^6$ compared with those of the threshold of 0.1 whose CSF number ranges from $(1.6-4.9) \times 10^5$. We therefore modified the energies obtained at the threshold of 0.1 by referring the more accurate energies with the threshold of 0.03 in order to design the analytical PES for the dynamics calculations. The modified PES is represented as

$$V_{mod}(R, r, \theta) = V_{CI>0.1}(R, r, \theta) + \Delta E(R, r, \theta) \qquad (2)$$

The PES was separated into two regions, $r \leq 1.8$ Å and $r \geq$

1.8 Å, to define the correcting term ΔE. The line $r = 1.8$ Å goes through the top of the potential barrier between the side-on and inserted complex. For the region $r \leq 1.8$ Å, ΔE was assumed to be a function of R and θ because this region is characterized by the approach of Ti to O_2 (see Figure 1). At $\theta = 90°$, we used the energies of four points (i.e., the reactant ($R \geq 4.0$ Å), the top of the entrance barrier ($R = 2.41$ Å), the side-on complex ($R = 1.62$ Å), and the barrier between the side-on and inserted complex ($R \leq 1.5$ Å)), which have correction energies of 0.0, −0.193, −0.297, and −0.517 eV, respectively. ΔE at an intermediate value of R was obtained by linear interpolation of these energies. At $\theta = 5°$, we used the energies of three points—those of the reactant ($R \geq 4.0$ Å), the top of the potential barrier ($R = 3.2$ Å), and the end-on complex ($R \leq 2.49$ Å) with correction energies of 0.0, −0.311, and −0.027 eV, respectively. The angle dependence of ΔE was assumed to have the form

$$\Delta E(R, r, \theta) = \frac{1}{1 + \cos 10°}\{(1 + \cos 2\theta)\, E(R, r, 5°) + (\cos 10° - \cos 2\theta)\, E(R, r, 90°)\} \quad (3)$$

that was derived by substituting the values at $\theta = 5°$ and 90° into the function $\Delta E(R, r, \theta) = a + b \cos 2\theta$. The region $r \geq 1.8$ Å includes the inserted complex and the dissociation pathway to the TiO and O products. We thus assumed that the correction term ΔE is independent of R. The correction energies at the inserted complex, −0.179 eV for $r = 2.79$ Å, and the product, 0.358 eV for $r \geq 4.0$ Å, as well as at the boundary between the two regions, $r = 1.8$ Å, were used for linear interpolation with respect to r. We used the same relation as in eq 3 to describe the angular dependence of ΔE in this region.

About 700 modified $^1A'$ MRCI energies thus obtained were used to construct the analytical PES. Because the TiO_2 PES with two deep minima separated by a low potential barrier is difficult to represent by a simple analytical function, we divided the PES into three regions and fit the energies at each region to a Murrell−Sorbie-type many-body expansion function[17] separately. The region I, $r \leq 1.8$ Å and $R \geq 2r - 0.25$ Å, containing the reactant and end-on complexes was represented by the function

$$V(R_1, R_2, R_3) = V^{(1)} + V^{(2)}_{OO}(R_1) + V^{(2)}_{TiO}(R_2) + V^{(2)}_{TiO}(R_3) + V^{(3)}(R_1, R_2, R_3) \quad (4)$$

where R_1 is the O−O distance and R_2 and R_3 are the Ti−O distances. The one-body term $V^{(1)}$ was taken to be zero because both the O_2 and TiO molecules dissociate into atoms in their ground states. The two-body terms (i.e., the diatomic potentials) were given by the extended Rydberg form

$$V^{(2)}(R) = -D_e(1 + a_1\rho + a_2\rho^2 + a_3\rho^3)\exp(-a_1\rho) \quad (5)$$

where $\rho = R - R_e$, with R_e being the equilibrium bond distance. For the O_2 molecule, the parameters D_e, R_e, ω_e, $\omega_e x_e$, and $\omega_e y_e$ were derived from the spectroscopic data[18]. For TiO, however, the parameter a_2 in eq 5 obtained in a similar way became negative, and the resultant potential energy showed nonphysical behavior at large R. We therefore carried out MRCI calculations for the TiO potential curve and fit the curve to eq 5. Because the present MRCI calculations gave a dissociation energy D_e of 6.11 eV, the ab initio energies were scaled so as to reproduce the experimental D_e of 6.93 eV. The harmonic frequency calculated from the present TiO function is 1004.5 cm^{-1}, which is in good agreement with the experimental value, $\omega_e = 1009.0$ cm^{-1}. The three-body term $V^{(3)}(R_1, R_2, R_3)$ is given by

$$V^{(3)}(R_1, R_2, R_3) = V^0 \sum_{i,j,k,=0}^{i+j+k\leq 5} C_{ijk}\rho_1^i\,\rho_2^j\,\rho_3^k \times (1 - \tanh\gamma_1 Q_1/2)(1 - \tanh\gamma_2 Q_2/2) \quad (6)$$

where

$$Q_1 = R_1 - R_1^0 \quad (7a)$$

and

$$Q_2 = (1/\sqrt{2})(R_2 + R_3 - R_2^0 - R_3^0) \quad (7b)$$

The polynomial in eq 6 was truncated after the fifth-order term. The potential parameters were determined by the least-squares fitting procedure to include about 260 modified MRCI energies V_{mod} in region I. Region III, $r \geq 1.8$ Å, covers the inserted intermediate and the product. We used the same two-body functions as were used for region I, and the three-body term was least-squares fitted to about 290 energies in region III.

For region II, $r \leq 1.8$ and $R \leq 2r - 0.25$ Å, where the number of grid points is about 160, the sum of two body terms of isolated O_2 and TiO molecules determined above was not a good approximation of the PES, and the three-body term became very large because the TiO internuclear distance of the side-on intermediate, 1.79 Å, is close to the TiO equilibrium bond length, 1.62 Å, in spite of the fact that there is no strong bonding between the Ti and O atoms. We therefore redefined the two-body terms for this region. The parameters for the TiO potential were determined by the least-squares fitting to the energy $V_{mod} - V^{(2)}_{OO}(R_1)$ where $V^{(2)}_{OO}$ is the diatomic potential of an isolated O_2 molecule. The modified TiO potential $V^{(2)'}_{TiO}$ thus obtained was used to obtain the modified O_2 potential, which was constructed by the least-squares fitting to the energy $V_{mod} - V^{(2)'}(R_2) - V^{(2)'}(R_3)$. The effective two-body potentials have smaller dissociation energies, 1.80 eV for TiO and 3.33 eV for O_2, than those of the isolated diatomic molecules, 6.93 and 5.21 eV, respectively. With these modified two-body functions, the fitting of the three-body term was improved considerably.

To construct the global PES, we combined the three potential functions as

$$V(R_1, R_2, R_3) = \{(1 - S_1)V_I + S_1V_{II}\}S_2 + (1 - S_2)V_{III} \quad (8)$$

where V_I, V_{II}, and V_{III} are the potential functions for regions I, II, and III, respectively. The switching functions are given by

$$S_1 = (^1/_2)(1 - \tanh(\gamma_1(\Delta r_1))) \quad (9a)$$

and

$$S_2 = (^1/_2)(1 - \tanh(\gamma_2(\Delta r_2))) \quad (9b)$$

where Δr_1 and Δr_2 are the distances of a point (R_1, R_2, R_3) measured from the dividing lines of the regions $R = 2r - 0.25$ Å for Δr_1 and $r = 1.8$ Å for Δr_2. The parameters γ_1 and γ_2 were determined by least-squares fits to the energies near the dividing lines $|\Delta r_{1,2}| < 0.2$ Å. Because the PES of TiO_2 contains several local minima and potential barriers, as seen in Figure 1, the fitting of the modified MRCI energies to an analytical function was a difficult task. The root-mean-square deviation, 0.16 eV, was thus large. The optimized potential parameters for the $1^1A'$ state are provided as Supporting Information.

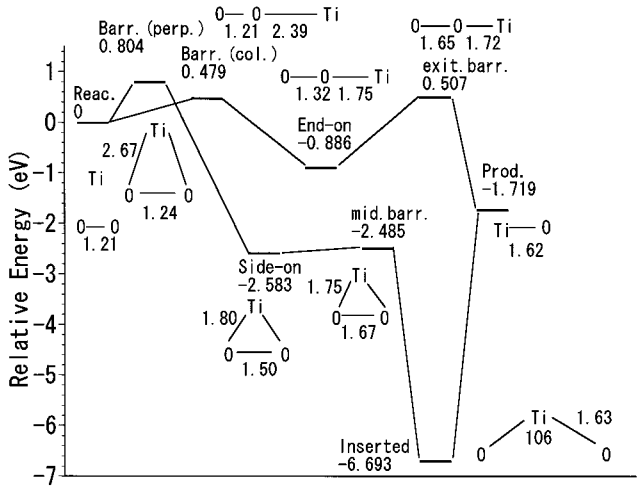

Figure 3. Geometries and energies of the stationary points for analytical PES.

The potential-energy profile derived from the analytical PES is shown in Figure 3. The global features are almost the same as those of the modified PES and of Figure 1. The geometries and energies of the side-on, inserted, and end-on intermediates are consistent with the MRCI results for the threshold of 0.03 in Table 1, though the O−O and Ti−O bond distances of the inserted complex become shorter for the analytical PES. The entrance barrier height increases by 0.13 eV from that of the MRCI both at $\theta = 0$ and 90°, and the location of the saddle point slightly shifted toward the direction of the end-on intermediate. We note that transition states with one imaginary frequency are the collinear entrance barrier and the middle barrier between the side-on and inserted intermediate in Figure 3, but the entrance barrier at the perpendicular geometry and the exit barrier from the end-on intermediate have two imaginary frequencies.

3. Classical Trajectory Calculation

We employed the standard QCT method[19] to study reaction 1. The initial separation between Ti and the center of mass of O_2 was chosen to be 6.0 Å. This separation ensures that the interaction energy can be neglected with respect to the energy of the reactant. The integration of the equations of motion was carried out by the fourth-order Runge−Kutta method with a time step of 0.05 fs, which guarantees that the error of the total energy constancy is less than 1×10^{-4} eV.

The initial vibrational quantum number of O_2 was taken to be zero, but the rotational quantum number was generated according to the Boltzmann distribution at 300 K. We chose four initial relative translational energies, $E_T = 0.55$, 0.6, 0.7, and 0.8 eV, that lie between the entrance barrier height at the collinear geometry, 0.48 eV, and at the perpendicular geometry, 0.80 eV, of the present analytical PES. The maximum value of the impact parameter b_{max} for reactive trajectories depends on E_T and increases from 1.07 Å at $E_T = 0.55$ eV to 1.89 Å at $E_T = 0.8$ eV. b_{max} was obtained from preliminary trajectory calculations. In the actual calculations, the impact parameter was randomly sampled so as to cover uniformly the area inside the circle $2\pi b_{max}$ for each value of E_T. A total of 10 000 trajectories were run for each initial translational energy to calculate the reactive cross section, but 50 000 trajectories with $E_T = 0.55$ eV were averaged to study the lifetime of the collision complex and the product energy distributions.

A. Rate Constant. We calculated the reactive cross section at four relative translational energies. The resultant cross sections

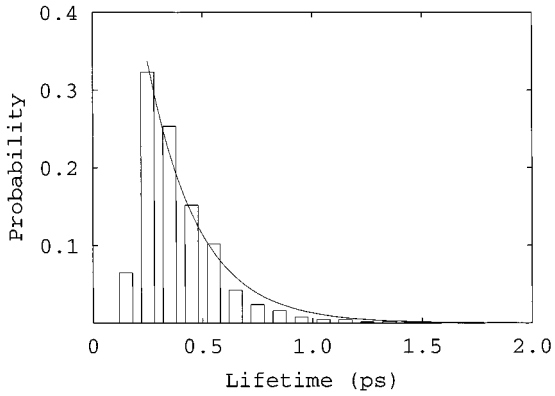

Figure 4. Distribution of the lifetime of the collision complex.

were 0.19, 0.60, 1.93, and 3.80 Å^2 for $E_T = 0.55$, 0.6, 0.7, and 0.8 eV, respectively, which was well-represented by the fourth order polynomial

$$\sigma(E_T) = 77.0(E_T - E^{\ddagger})^4 - 84.5(E_T - E^{\ddagger})^3 + 59.7(E_T - E^{\ddagger})^2 \quad (10)$$

where $E^{\ddagger}$ is the entrance barrier height for the analytical PES, 0.479 eV.

The thermal rate constant at $T = 300$ K was calculated by

$$k(T) = (2/k_B T)^{3/2}(\pi\mu)^{-1/2}\int_0^{\infty} \sigma(E_T)\exp(-E_T/k_B T)E_T\,dE_T \quad (11)$$

where k_B is the Boltzmann constant and μ is the reduced mass of the reactant pair. Because the collinear entrance barrier height is overestimated by 0.135 eV relative to the MRCI value, as mentioned in section 3, we replaced the value of $E^{\ddagger}$ in eq 10 by 0.344 eV before calculating the rate constant. The rate constant was calculated to be 1.2×10^{-17} cm^3/s, which is much lower than the experimental estimate reported by Ritter and Weisshaar, $(1.5 \pm 0.3) \times 10^{-12}$ cm^3/s. The discrepancy between the experimental rate constant and the present one is apparently attributed to the overestimation of the entrance barrier height in the present PES.

In estimating the activation energy, Ritter and Weisshaar employed the prefactor $A = \sigma_{HS}\langle v\rangle = 2.5 \times 10^{-10}$ cm^3/s where σ_{HS} is the hard-sphere collision cross section. As shown in section 3, the entrance barrier height depends on the orientation angle of Ti with respect to the O_2 molecular axis, thus the prefactor should be smaller than that of the hard-sphere model. We estimated the prefactor to be 7.2×10^{-12} cm^3/s using the calculated rate constant and the barrier height. Combining the present value of the prefactor with the experimental rate constant, the activation energy is estimated to be 0.9 kcal/mol, which is still smaller than the experimental estimate, 3.1 kcal/mol.

B. Reaction Mechanism. To explore the dynamics of reaction 1, we have examined the records of 2700 reactive trajectories at $E_T = 0.55$ eV. Figure 4 shows the lifetime distribution of the TiO_2 collision complex, which is the time that the complex is trapped in the intermediate potential wells. The lifetime of a trajectory was defined as the period between the time of passing through the entrance barrier and the time when one of the TiO bond distance is twice as large as the other. As seen in Figure 4, the number of trajectories that react within 0.2 ps is very small, though about 80% of the trajectories dissociate to the product TiO + O within 0.5 ps. The average lifetime is calcualted to be 0.39 ps. Beyond 0.2 ps, the

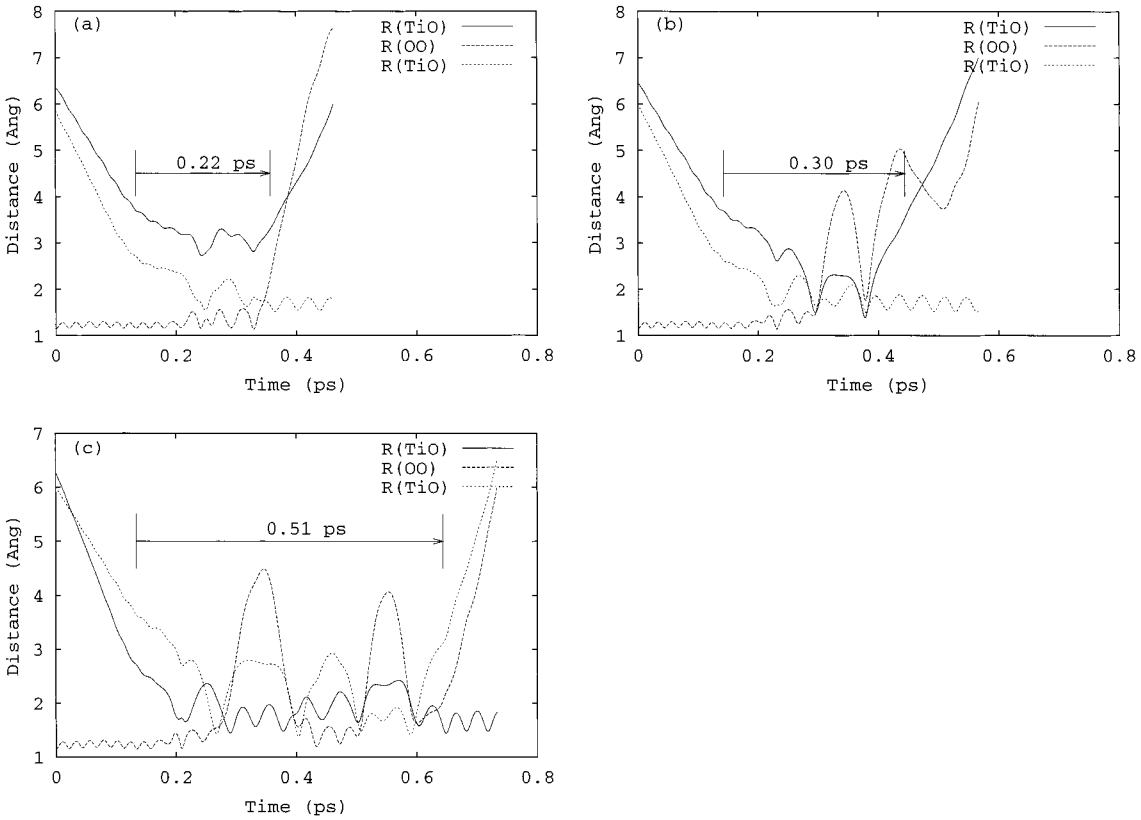

Figure 5. Time evolution of the internuclear distances (R_{OO}, R_{TiO}) for three representative trajectories.

distribution can be well-represented by a single-exponential function $\exp(-t/\tau)$ with $\tau = 0.23$ ps. A relatively short lifetime of the collision complex is attributed to a large excess energy in the collision complex.

Analyses of the time evolution of the interatomic distances and potential energy of the trajectories were performed. All the reactive trajectories occurred near the collinear geometry in the region of the entrance barrier because the translational energy, 0.55 eV, is close to the energy of the transition state, 0.48 eV, and the trajectories with a large value of θ cannot overcome the energy of this entrance barrier. Figure 5 displays the evolution of interatomic distances for three typical trajectories. Figure 5a shows an example of the direct abstraction mechanism where the Ti atom approaches one of the O atoms collinearly and abstracts the O atom without forming the side-on or inserted reaction intermediates. The lifetime of this trajectory is very short, 0.22 ps. However, the contribution of the abstraction mechanism to the reactive cross section is very small because the end-on complex is unstable with respect to the bending of the Ti−O−O angle, and a more stable side-on or inserted complex is easily formed. This result is consistent with the lifetime distribution in Figure 4, where the probability of short lifetime trajectories within 0.2 ps is very small.

Most of the reactive trajectories proceed via the inserted mechanism. A trajectory evolving through the inserted complex and dissociating quickly is illustrated in Figure 5b. In this type of trajectory, the Ti−O bond is first formed and then broken because of the impulsive force acting at the repulsive wall between the Ti and O atoms. Thus, the lifetime of this trajectory is short, 0.30 ps. Because the kinetic energy is large in the collision complex, this insertion/fast dissociation mechanism is important in interpreting many reactive trajectories. We also found trajectories that survive for a long time in the reaction intermediates, the insertion/slow dissociation mechanism. Such a trajectory is shown in Figure 5c where both the side-on and inserted complexes are formed (0.3−0.6 ps), followed by dissociation to the product. In these trajectories, the Ti−O bond initially formed in the end-on complex does not necessarily dissociate, and the intramolecular vibrational energy redistribution occurs to some extent.

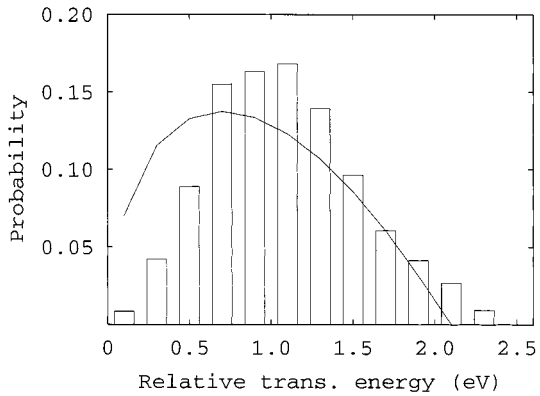

Figure 6. Distribution of the relative translational energy of the products. The solid line is the prior distribution.

C. Product Energy Distributions. We calculated the product translational, rotational, and vibrational energy distributions and compared them with the statistical distributions (i.e., the a priori distributions[20]). Although we considered only the case in which the initial translational energy was 0.55 eV, the product energy distributions are expected to be insensitive to the initial energy because the reaction is strongly exothermic, 1.72 eV, and there is no exit-channel barrier. Figure 6 shows the distribution of the relative translational energy between the products TiO and O. The peak at 1.1 eV for the trajectory result is higher than that of the statistical distribution, and the probability in the small energy region is lower. The average translational energy is 1.08 eV, which is 46% of the available product energy, 2.33 eV.

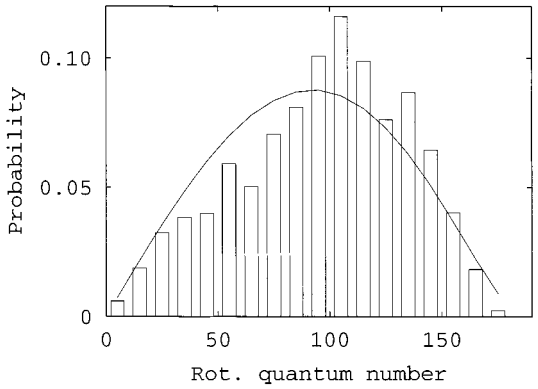

Figure 7. Distribution of the rotational quantum number of TiO. The solid line is the prior distribution.

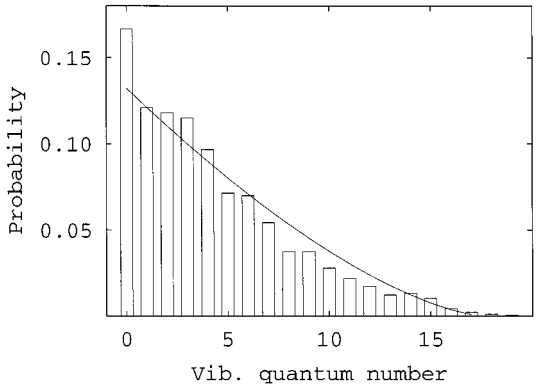

Figure 8. Distribution of the vibrational quantum number of TiO. The solid line is the prior distirbution.

Note that the statistical theory predicts an average translational energy of 1.00 eV.

The distribution of the rotational quantum number j is plotted in Figure 7, where we can see that the rotational distribution has its maximum at $j \approx 105$. As in the case of the relative translational energy, the probability of low rotational energy below $j = 90$ is smaller than the statistical probability, indicating that the product rotation is greater than that expected from the statistical assumption. The average rotational energy is calculated to be 0.71 eV, which is 30% of the available product energy. The vibrational quantum number distribution of TiO is shown in Figure 8. The probability monotonically decreases from $v' = 0$ and becomes zero at $v' = 20$. Compared with the statistical distribution, the trajectory calculations gave a larger probability at $v' = 0$ and smaller one for $v' \geq 7$. Thus, the average vibrational energy, 0.58 eV, is smaller than the statistical energy, 0.67 eV.

The product energy distributions in Figures 6−8 may be regarded as rather statistical, which is consistent with the inserted reaction mechanism mentioned above. A slightly hot distribution of the translational and rotational energies is attributed to the short lifetime of the collision complex because of the large excess energy measured from the bottom of the potential well of the inserted complex. We note that there is no available experimental data for the product energy distributions for reaction 1. Experimental studies to measure them would provide detailed information about the reaction mechanism.

Although the present PES overestimates the entrance barrier height, its effect on the product energy distributions will be small because the present reaction is highly exothermic.

4. Conclusions

We have studied the oxidation reaction of ground-state Ti with O_2 theoretically. The global PESs for the $1^1A'$ and $1^3A'$ states were calculated at the MRCI level. The PES features of both of the electronic states were similar; there exist deep potential wells corresponding to the side-on and inserted intermediate complexes, and the entrance barrier height leading to the end-on complex was comparable for both the states. We constructed an analytical PES function for the $1^1A'$ state on the basis of more than 700 ab initio energies modified by more elaborate MRCI calculations with a smaller threshold for the configuration selection. The derived analytical PES reproduced well the characteristics of the ab initio surface, though the entrance barrier height was slightly overestimated.

QCT calculations were carried out to estimate the reaction rate, the lifetime of the collision complex, and the product energy distributions. The calculated rate constant is smaller than the experimental value, which is attributed to the overestimation of the entrance barrier height of the present PES. Using the prefactor obtained from the present QCT calculations combined with the experimental rate constant, the true activation energy is estimated to be 0.9 kcal/mol, which is lower than the experimental estimate, 3.1 kcal/mol, obtained assuming the hard-sphere collision model. Detailed analyses of trajectories revealed that the reaction can be described by the inserted/fast dissociation mechanism, which is consistent with the short average lifetime of the collision complex, 0.39 ps. The product translational, rotational, and vibrational energy distributions were similar to those of the statistical assumption. However, the translational and rotational energies are slightly hotter than those obtained from the statistical prediction, but the probability of $v' = 0$ for the TiO vibration is larger than the statistical value, reflecting the fact that the reaction proceeds via the insert/fast dissociation mechanism involving a short-lived collision complex. Experimental measurements of the lifetime of the collision complex and the product energy distributions will provide valuable information for the study of the reaction mechanism.

Although the present study provides important insight into the oxidation of Ti by O_2, achieving full understanding of the reaction mechanism would require more elaborate studies to be carried out. As mentioned in section 2, the triplet state can participate to the reaction. To obtain information about the contribution of triplet channels, more accurate calculations of the PESs are necessary. We also note that we neglected the excited electronic states in the singlet manifold in the present treatment. The transition to the excited electronic states may become important when the initial translational energy is large because of the crossing of PESs between the 1^1B_2 and 1^1A_1 states in the entrance barrier region for the perpendicular approach of Ti to O_2.

Finally, we point out that TiO_2 is very difficult to understand theoretically, and even higher-level calculations would be useful in the future. The present work can be regarded as a starting point for future studie.

Acknowledgment. This work was supported by the Grant in Aid for Scientific Research from the Ministry of Education and Science, Japan.

Supporting Information Available: Parameters of two- and three-body terms and of switching functions. This material is available free of charge via the Internet at http://pubs.acs.org.

References and Notes

(1) Ritter, D.; Weisshaar, J. C. *J. Phys. Chem.* **1989**, *93*, 1576.
(2) Ritter, D.; Weisshaar, J. C. *J. Phys. Chem.* **1990**, *94*, 4907.

(3) Clemmer, D. E.; Honma, K.; Koyano, I. *J. Phys. Chem.* **1993**, *97*, 11480.
(4) Haynes, C. L.; Honma, K. *J. Chem. Soc., Faraday Trans.* **1998**, *94*, 171.
(5) Honma, K. *J. Phys. Chem. A* **1999**, *103*, 1809.
(6) Matsui, R.; Senba, K.; Honma, K. *Chem. Phys. Lett.* **1996**, *250*, 560.
(7) Matsui, R.; Senba, K.; Honma, K. *J. Phys. Chem. A* **1997**, *101*, 179.
(8) Blomberg, M. R. A.; Siegbahn, P. E. M.; Strich. A. *Chem. Phys.* **1985**, *97*, 287.
(9) Pápai, I.; Mascetti, J.; Fournier, R. *J. Phys. Chem. A* **1997**, *101*, 4465.
(10) Stirling, A. *J. Phys. Chem. A* **1998**, *102*, 6565.
(11) Werner, H.-J.; Knowles, P. J. *J. Chem. Phys.* **1988**, *89*, 5803.
(12) Wachters, A. J. H. *J. Chem. Phys.* **1970**, *52*, 1033.
(13) Hay, P. J. *J. Chem. Phys.* **1977**, *66*, 4377.
(14) Dunning, T. H.; Hay, P. J. In *Modern Theoretical Chemistry*; Schaefer, H. F., Ed.; Plenum Press: New York, 1977; Vol. 3.
(15) MOLPRO is a package of ab initio programs written by Werner, H.-J.; Knowles, P. J. with contributions from Almöf, J; Amos, R. D.; Berning, A.; Cooper, D. L.; Deegan, M. J. O.; Dobbyn, A. J.; Eckert, F.; Elbert, S. T.; Hampel, C.; Lindh, R.; Lloyd, A. W.; Meyer, W.; Nicklass, A.; Peterson, K.; Pitzer, R.; Stone, A. J.; Taylor, P. R.; Mura, M. E.; Pulay, P.; Schütz, M.; Stoll, H.; Thorsteinsson, T.
(16) Ramana, M. V.; Phillips, D. H. *J. Chem. Phys.* **1988**, *88*, 2637.
(17) Murrell, J. H.; Carter, S.; Farantos, S. C.; Huxley, P.; Varandas, A. J. C. *Molecular Potential Energy Functions*; Wiley & Sons: Chichester, 1984.
(18) Huber, K. P.; Herzberg, G. *Constants of Diatomic Molecules;* Van Nostrand: Princeton, 1979.
(19) Truhlar, D. G.; Muckerman, J. T. In *Atom−Molecule Collision Theory: A Guide for the Experimentalist;* Bernstein, R. B., Ed.; Plenum Press: New York, 1979.
(20) Levine, R. D. *Theory of Chemical Reaction Dynamics;* Baer, M., Ed.; CRC Press: Boca Raton, FL, 1985; Vol 4.